MoS_2-OH Bilayer Mediated Growth of Inch-Sized Monolayer MoS_2 on Arbitrary Substrates

Juntong Zhu[1,‡], Hao Xu[2,‡], Guifu Zou[1,*], Wan Zhang[1], Ruiqing Chai[3], Jinho Choi[1], Jiang Wu[2,*], Huiyun Liu[2], Guozhen Shen[3], Hongyou Fan[4,5,*]

[1]College of Energy, Soochow Institute for Energy and Materials Innovations, and Key Laboratory of Advanced Carbon Materials and Wearable Energy Technologies of Jiangsu Province Soochow University, Suzhou 215006, China; [2]Department of Electronic and Electrical Engineering, University College London, Torrington Place, London WC1E 7JE, UK; [3]State Key Laboratory for Superlattices and Microstructures, Institute of Semiconductors, Chinese Academy of Sciences, Beijing 100083, China; [4]Center for Integrated Nanotechnology, Sandia National Laboratory, Albuquerque, NM 87185, United States [5]Chemical and Biological Engineering, Center for Micro-Engineered Materials, University of New Mexico, Albuquerque, NM 87122, United States.

KEYWORDS: monolayer, MoS_2, inch-size, electronics, nanocrystals, 2D materials.

ABSTRACT: Due to remarkable electronic property, optical transparency and mechanical flexibility, monolayer molybdenum disulfide (MoS_2) has been demonstrated to be promising for electronic and optoelectronic devices. To date, the growth of high-quality and large-scale monolayer MoS_2 has been one of the main challenges for practical applications. Here we present a MoS_2-OH bilayer mediated method that can fabricate inch-sized monolayer MoS_2 on arbitrary substrates. This approach relies on a layer of hydroxide groups (-OH) that are preferentially attached to the (001) surface of MoS_2 to form MoS_2-OH bilayer structure for growth of large area of monolayer MoS_2 during the growth process. Specifically, the hydroxide layer impedes vertical growth of MoS_2 layers along the [001] zone axis, promoting the monolayer growth of MoS_2, constrains growth of the MoS_2 monolayer only in lateral direction into larger area, and effectively reduces sulfur vacancy and defects according to density functional theory calculations. Finally, the hydroxide groups advantageously prevent the MoS_2 from interface oxidation in air, rendering high-quality MoS_2 monolayers with carrier mobility up to ~ 30 $cm^2\ V^{-1}\ s^{-1}$. Using this approach, inch-sized uniform monolayer MoS_2 has been fabricated on the sapphire and mica and high-quality monolayer MoS_2 of single crystalline domains exceeding 200 μm has been grown on various substrates including amorphous SiO_2 and quartz and crystalline Si, SiC, Si_3N_4 and graphene This method provides a new opportunity for the monolayer growth of other two-dimensional (2D) transition metal dichalcogenides (TMDs) such as WS_2, $MoSe_2$.

INTRODUCTION

2D TMDs have drawn extensive attention due to their attractive physical properties, such as outstanding electronic property, optical transparency, and mechanical flexibility.[1-5] It was demonstrated that TMD semiconductors undergo an indirect-to-direct band gap transition when thinned from bulk to a monolayer.[1] Monolayer molybdenum disulfide (MoS_2) is a representative TMD with a direct bandgap, and has been widely studied for applications in field effect transistors (FETs), photodetectors, piezotronic devices, *etc*.[5-9] The growth of high-quality and large-scale monolayer MoS_2 underpins these technological advancements. Among various methods, the CVD approach has the potential for scaled-up production of high-quality 2D materials.[5, 10-16] However, monolayer MoS_2 growth has still suffered from a high defect density, small domain size and formation of multilayers because of non-uniformity of aggregated/diffusing precursors on growth substrates and nucleation of crystallites occurred preferentially at impurities or defect sites on solid substrates. They prevent the full potential of monolayer MoS_2 to be realized.[17-19] Therefore, the key step is to find a substrate-independent strategy for the growth of high quality monolayer MoS_2.

Herein, we report a MoS_2-OH bilayer mediated method for fabrication of inch-sized monolayer MoS_2 on arbitrary substrates. This method demonstrates that hydroxide (-OH) groups in the aqueous solution are preferentially attached to the (001) surface of MoS_2 during the growth process. They not only suspend the growth along the [001] zone axis which promotes formation of monolayer MoS_2, but also lead to a lower density of sulfur vacancies and defects. According to density functional theory (DFT) calculations, the -OH surface groups are proved to drive the growth of monolayer MoS_2 on arbitrary susbtrates. Inch-sized uniform monolayer MoS_2 can be obtained on both sapphire and mica substrates. More importantly, high-quality monolayer MoS_2 with domain size exceeding 200 μm can be grown on various substrates, from crystalline Si, SiC, Si_3N_4, and graphene to amorphous SiO_2 and quartz.

EXPERIMENTAL

Substrate Preparation: To improve the wettability of molybdenum precursor during spin coating, the surface of various

substrates was transformed from weakly hydrophilic to hydrophilic by treating with piranha solution (Be cautious: H_2O_2 and H_2SO_4 in the ratio of 2:3). After the piranha treatment, the substrates were rinsed with copious amounts of deionized water and dried with the N_2 gun.

Preparation of hydroxide-assisted aqueous solution: 0.05 g ammonium molybdate (powder, 98 %) and different proportions of KOH were dissolved in 5 mL deionized water to obtain 0, 0.25, 1 and 4 M KOH precursor solutions, respectively. Those precursor solutions were then spin coated to diverse substrates with 8000 rpm/s to obtain a well-distributed film.

Growth of monolayer MoS_2: An alumina boat loaded with several spin-coated substrates was placed at the heating center of a quartz tube, and another alumina boat loaded with 50 mg sulfur at the upstream of the tube, where the temperature was independently controlled. Then the center of quartz tube was ramped up to 750 °C for 40 min, meanwhile the S powder was heated to 200 °C for 15 min. Growth of MoS_2 was carried out at 750 °C under inert atmosphere (30 sccm Ar) for 10 min. then the furnace was naturally cooled to room temperature.

***In situ* TEM observation:** The TEM samples were spin-coated with 1 M and without KOH precursor solution on a Si_3N_4 membrane (Si_3N_4 thickness of ~50 nm) supported by a silicon E-Chip, respectively. The TEM observations were conducted in a Cs-corrected environmental TEM (FEI, Titan ETEM, 300 kV). During the observations, the sample was irradiated with the intensity of the e-beam ~200 pA cm^{-2}, and the image was recorded with a Gatan SC1000 ORIUS CCD camera with a short exposure time (~1 s).

Transfer of monolayer MoS_2: i) 9 g of PS with a molecular weight of 280000 g/mol was dissolved in 100 mL of toluene and then the PS solution was spin-coated (3500 rpm for 60 s) on as-grown monolayer MoS_2 on any substrates. ii) the sample was baked at 80 °C for 15 min. iii) A water droplet was dropped on top of the sample, resulting in the delamination of the PS-MoS_2 assembly. iv) the floating PS-MoS_2 film was dredged up with a clean SiO_2/Si substrate or a holeycarbon TEM grid. v) a mild baking at 80 °C for 1 h to remove the water residues and a final baking for 30 min at 150 °C to spread the polymer for the elimination of possible wrinkles. vi) PS was removed by rinsing with toluene several times.

Structure and optical property characterization: The morphology of the as-grown MoS_2 was characterized using an optical microscope (Nikon Eclipse LV100) and SEM (FEI Scios, 15 kV). The phase of products was checked by using an XRD (Bruker D8 Advance). X-ray photoelectron spectroscopy (Thermo Fisher Escalab 250Xi) was used to characterize the chemical composition of as-grown MoS_2 sample with -OH. HRTEM imaging was performed on a field emission TEM (FEI Tecnai F20, 200 kV); SAED measurements were performed on a TEM operating at 120 kV (FEI Tecnai T12). Room temperature ADF-STEM imaging was performed using a JEOL ARM200F at 200kV. Raman and PL spectra/maps were collected with a confocal Raman spectrometer (Horiba Jobin Yvon HR Evolution) using a 532-nm laser as the excitation source. The laser spot size was 1 mm and the laser power on the sample surface was kept below 60 mW.

AFM and KPFM Measurement: The AFM and KPFM images were obtained using a Bruker Dimension Icon AFM system. An AFM tip (SCANASYST-AIR, Bruker Nano Inc.) was applied to probe the topography and thickness of the samples in the peak-force working mode, while the KPFM measurements were performed using a conductive tip (SCM-PIT-V2, Bruker.) with a resonant frequency of 75 kHz, a lift height of 60 nm, and the ac bias of 0.5 V. To obtain quantitative work function values of as-grown MoS_2, we calibrated the tip on the gold surface by using the known work function of gold φ_{Au} = 5.10 eV. The work function of as-grown monolayer MoS_2 can be calculated using the following equations: $\phi_{tip} = 4.765$ eV,

$$\phi_{substrate} = \phi_{tip} - e\left(CPD_{tip} - CPD_{substrate}\right) = 4.765 - 0.045 = 4.72 \text{ eV},$$

$$\phi_{MoS_2} = \phi_{substrate} + e\Delta DP = 4.72 - 0.07 = 4.65 \text{ eV}.$$

Density functional theory calculations: The first-principles DFT calculations were carried out by using the projector-augmented wave (PAW)[20] method and the Perdew-Burke-Ernzerhof exchange correlation functional[21-22] as implemented in the Vienna Ab-initio Simulation Package (VASP).[23] To include the effects of van der Waals interactions, the approach of Grimme (DFT-D3)[24] was adopted. The calculated equilibrium lattice constants are a = b = 3.15180 Å and c = 17.94945 Å for bulk MoS_2 and a = 4.77805 Å for α-Al_2O_3 (Sapphire). The cutoff energy for the plane-wave basis set is 500 eV. The α-Al_2O_3(001) surface was simulated by a twelve-layer *p* (2×2) unit cell containing 80 atoms, with a vacuum region of 15 Å. Here the surface is Al-terminated, which is known as the most stable configuration.[25] The monolayer MoS_2 deposited on α-Al_2O_3(001) were simulated by a (3×3) unit cell: the lattice mismatch is ~1.0%. The surface Brillouin zone was sampled using a 15×15×1 *k*-point mesh. All the atoms except the bottom five atomic layers of α-Al_2O_3 (001) were allowed to relax until the forces exerted on each atom are less than 0.02 eV/Å, while the bottom five layers were fixed in their respective bulk positions. The adsorption energies of OH^- were calculated by using neutral systems with a homogeneous background charge, as described in a previous DFT study.[26]

Electrical Characterization: Monolayer MoS_2 were transferred to n-doped Si substrates with 300-nm-thick SiO_2. Subsequently, a conventional photolithography was used to pattern the source and drain electrodes, followed by a thermal evaporation and lift-off process to achieve Ni/Au electrodes with a thickness of 10 nm/50 nm. All the current–voltage (I–V) characteristics of the devices were measured with a Keithley 4200 semiconductor characterization system under ambition environment.

RESULTS AND DISCUSSION

The growth of monolayer MoS_2 was carried out by forming -OH groups via a solution spin-coating process as depicted in **Figure 1a-b and Figure S1**. Ammonium molybdate ($(NH_4)_2MoO_4$) was used as the Mo source and sublimed sulfur as the S source. Firstly, KOH (or NaOH) and $(NH_4)_2MoO_4$ were dissolved in deionized water to obtain an aqueous solution for generation of -OH groups The precursor solution was spin-coated to a sapphire substrate that was pretreated by a piranha solution to possess good hydrophilicity for a well-distributed precursor film with -OH formed on the sapphire.[27] Afterwards, the as-prepared sapphire substrates were annealed in a furnace tube. **Figure 1a** shows the Mo and S atoms are crystalized layer by layer at 750 ˚C without -OH. When introduced OH^- groups from aqueous solution, during the thermal annealed growth process, -OH groups are attached to the MoS_2 (001) surface, forming an S-Mo-S-OH bilayer structure. Further growth of MoS_2 along the [001] zone axis is suspended by

the surface -OH layer, which leads to preferential formation of a MoS_2 monolayer in the lateral direction instead of forming multilayers along the [001] axis. Under the constraint of the

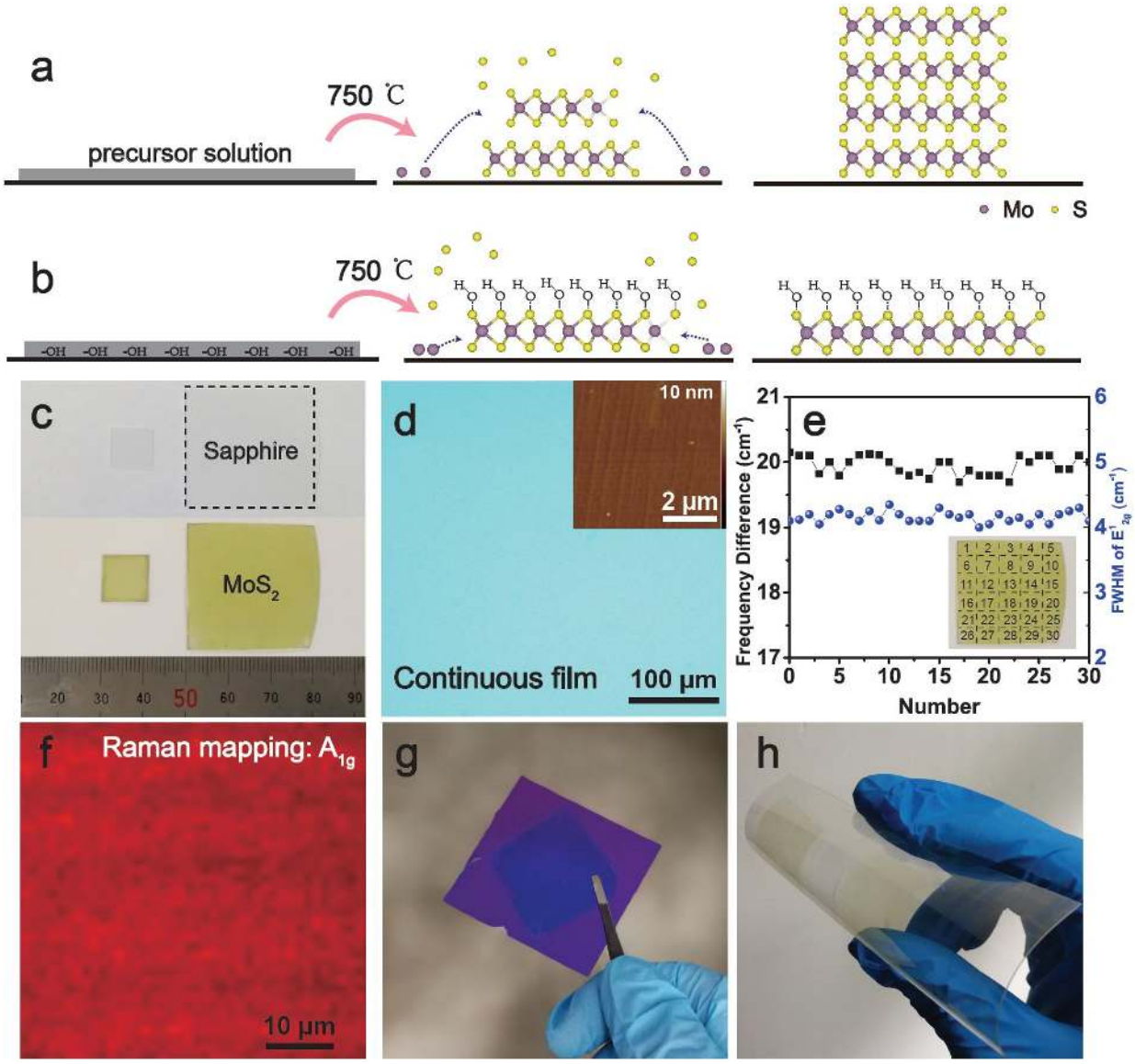

Figure 1. MoS_2 growth process in a precursor solution (a) without -OH and (b) with -OH. (c) Photographs of 1×1 and 3×3 cm^2 MoS_2 monolayer films on sapphire. (d) Typical OM image of a continuous MoS_2 film grown on sapphire. The inset is an AFM image, displaying an atomic-flat surface. (e) The statistical Δ (left y-axis) and FWHM (right y-axis) values of the E^1_{2g} peak plotted as a function of numbered sites in the 3×3 cm^2 MoS_2 film (inset photograph). The Δ and FWHM values of each site were extracted from the respective Raman spectrum, which was obtained from the central dot of each site. (f) Raman intensity mapping for A_{1g} peak of the as-grown monolayer MoS_2. (g, h) Photographs of the inch-size MoS_2 films transferred onto a SiO_2/Si substrate and a flexible PET substrate, respectively.

surface layer of -OH groups anchored on the MoS_2 (001) surface, Mo and S atoms can only attach to the edges of the monolayer MoS_2. As a result, monolayer MoS_2 grows only in lateral direction into larger area (**Figure 1b**). Figure 1c shows representative uniform MoS_2 monolayers that are grown with 100% coverage on 1×1 and 3×3 cm^2 sapphire using the surface -OH groups assisted method, and the transparent sapphire substrate becomes light brown after growth of the MoS_2 monolayer (**Figure 1c**). Optical microscopy (OM) and atomic force microscopy (AFM) images in **Figure 1d** show that the sapphire is completely covered by a uniform and atomically flat MoS_2 film with a surface roughness of ~ 0.12 nm. The layer thickness of the MoS_2 film was determined by Raman spectroscopy. The peaks of E^1_{2g} and A_{1g} in Raman spectra originate from in-plane and out-of-plane phonon modes, respectively.[28-29] Each phonon oscillation is sensitive to the thickness of MoS_2, and the Raman shift difference between the E^1_{2g} and A_{1g} modes depends on the layer numbers of MoS_2, which is about 20 cm^{-1} for monolayer MoS_2 and 25 cm^{-1} for bulk MoS_2.[30] In **Figure S2**, the characteristic Raman peaks obtained from the randomly selected site in MoS_2 monolayer are located at 384.3 cm^{-1} and 404.6 cm^{-1}, corresponding to E^1_{2g} and A_{1g} Raman modes, respectively. The specific frequency difference between the two peaks (Δ) is 20.3 cm^{-1}, suggesting the monolayer nature, and the narrow full width at half maximum (FWHM) ~ 4 cm^{-1} of the E^1_{2g} peak indicates a very low defect density of the as-

grown monolayer MoS_2 film.[28] The statistical analysis for Δ and FWHM values of the E^1_{2g} peak, both obtained from the numbered 30 sites, is shown in **Figure 1e**, demonstrating a good film uniformity across the entire sapphire. In addi

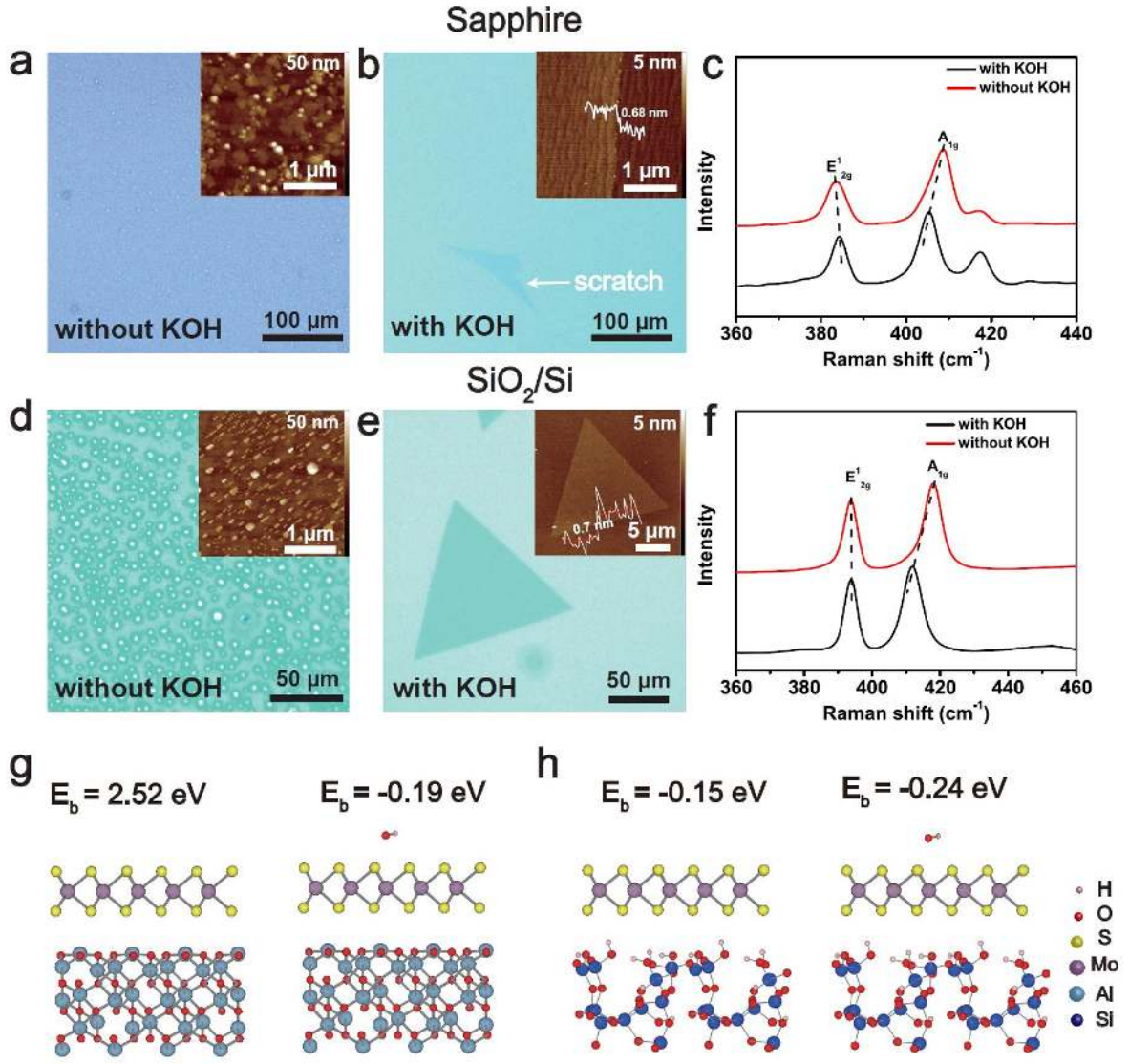

Figure 2. Critical role of the surface -OH groups in growth of monolayer MoS_2. OM and AFM images of MoS_2 grown on sapphire (a) without and (b) with -OH, respectively. The inset AFM image in (b) shows that the MoS_2 film thickness is ~ 0.68 nm, corresponding to the monolayer thickness. (c) The Raman spectra of MoS_2 films grown without and with -OH on sapphire. OM and AFM images of MoS_2 grown on SiO_2 (d) without and (e) with -OH, respectively. (f) The Raman spectra of MoS_2 films grown without and with -OH on SiO_2. The optimized structures of monolayer MoS_2 on (g) sapphire (001) and (h) amorphous SiO_2 substrates, together with the calculated binding energy (E_b) in the absence (left) and presence (right) of -OH, respectively.

tion, Raman intensity mapping of the A_{1g} band of a 50 × 50 μm^2 square area (**Figure 1f**) also manifests a uniform color contrast, further demonstrating the high degree of uniform spectroscopic quality of the resultant MoS_2 monolayer. After achieving large-scale monolayer MoS_2, transferring them is of much importance for the practical applications. Current transfer methods predominantly use poly (methyl methacrylate) (PMMA) as the supporting layer and NaOH or KOH solution bath is used to etch the substrate to separate the films, which may severely damage the film and substrate.[30-31] Thanks to the growth of hydrophobic MoS_2 films on hydrophilic substrates,[32] the inch-size monolayer MoS_2 can be readily transferred to arbitrary substrates without etching the growth substrates. As shown in **Figure 1g and h**, the inch-size monolayer MoS_2 was transferred to SiO_2/Si and polyethylene terephthalate (PET) substrates from sapphire by a polystyrene (PS)-assisted method. Notably, the PS-assisted method effectively avoided the damages caused by chemical etchants, so the transferred films on SiO_2/Si and PET well preserved their original quality. Meanwhile, the growth substrates avoided unnecessary contamination and irreversible damage. Indeed, as presented by the photographs and Raman spectra in **Figure S3**, the sapphire substrate was reused to grow high-quality and inch-size monolayer MoS_2 for multiple times.

To verify the critical role of the surface -OH layer in the growth of large-scale monolayer MoS_2, we compared MoS_2 samples grown on sapphire and SiO_2 substrates treated with-

out and with -OH (1 M KOH), respectively. The MoS_2 sample grown on sapphire without -OH (**Figure 2a**), shows many multilayers and small MoS_2 domains with average side length of ~ 500 nm. It is ascribed to the absence of surface

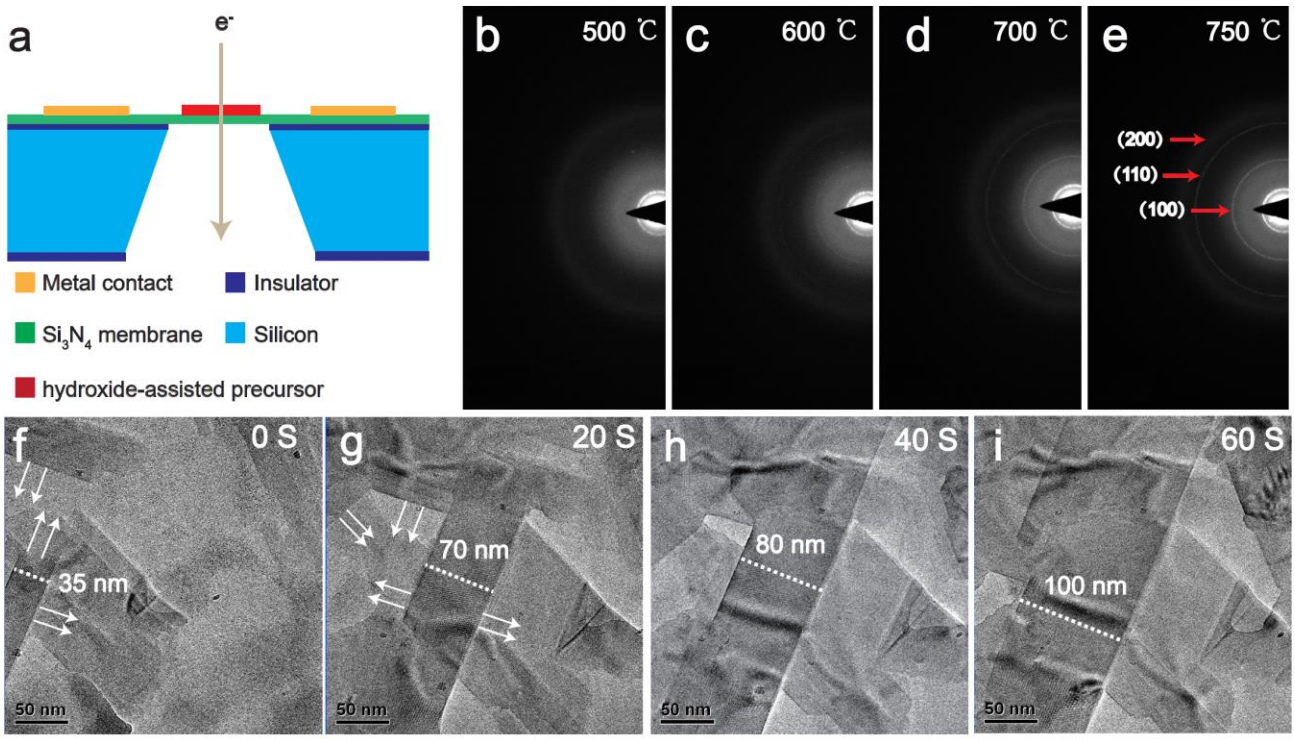

Figure 3. (a) Schematic side view of the experimental set-up of *in situ* TEM heating stage. (b - e) The evolution of SAED patterns across a temperature range: (b) 500 ℃, (c) 600 ℃, (d) 700 ℃ and (e) 750 ℃. (f - i) Time-resolved TEM images of the horizontal growth of MoS_2 at 750 ℃. (f) 0 s, (g) 20 s, (h) 40 s and (i) 60 s. Sequences of *in situ* TEM images display the controlled growth orientation of MoS_2 in the horizontal direction.

-OH groups that block the attachment of subsequent Mo and S atoms on the (001) surface, and thus, MoS_2 flakes were grown into multilayer and smaller islands.[33-34] In contrast, the MoS_2 monolayer film grown in the S-Mo-S-OH mode, completely and uniformly covers the sapphire substrate (**Figure 2b**). The AFM height profile of MoS_2 film with a scratch shows a thickness of ~ 0.68 nm, which is a typical monolayer thickness. The characteristic Raman spectra of MoS_2 grown on sapphire without and with -OH are shown in **Figure 2c.** Δ was measured to be 20.5 and 25 cm^{-1} for the MoS_2 grown without and with -OH (1 M KOH), respectively, further confirming the distinct advantage of forming S-Mo-S-OH structure when growing monolayer MoS_2. To exclude the substrate induced influences on the growth, we also performed growing monolayer MoS_2 on SiO_2, a typical amorphous substrate. Similarly, the growth carried out without -OH displays multilayer configuration and small MoS_2 flakes (**Figure 2d**). The inset AFM image shows a lot of multilayer islands and average side length of ~ 250 nm. Nevertheless, the MoS_2 sample grown with KOH shows large-scale monolayer domains with a large lateral size (~ 150 μm). The inset AFM image in **Figure 2e** shows a clean and flat surface of the triangular domain, confirming the monolayer nature of the domain (thickness ~ 0.7 nm). The monolayer MoS_2 keeps good uniformity in thickness, which is evidenced by both the Raman intensity map of A_{1g}peak and the photoluminescence map from the A-exciton (**Figure S4a-b**). The typical Raman spectra (**Figure 2f**) verify the forming the monolayer S-Mo-S-OH structure. To gain further insight into the key role of -OH groups, we performed density function theory (DFT) calculations for monolayer MoS_2 crystalized on single-crystalline sapphire and amorphous SiO_2 substrates (**Figure 2g, h**). For sapphire substrate, the calculated binding energy of MoS_2 in the absence of –OH is 2.52 eV that is much larger than -0.19 eV in the presence of -OH, indicating that the addition of -OH substantially stabilizes the monolayer MoS_2. It is noticeable that the deposition process of MoS_2 is converted from endothermic to exothermic by inclusion of -OH, which explains the hydroxide driven growth of monolayer MoS_2 observed in our experiments. For the amorphous SiO_2 substrate, the corresponding binding energy of MoS_2 in the absence of -OH is -0.15 eV that is higher than -0.24 eV in the presence of -OH, confirming that -OH further stabilizes the monolayer MoS_2. In addition, the formation of a hydroxide-covered MoS_2 is energetically favorable: the formation energy is -0.24 eV per (1×1) MoS_2, which is consistent with the formation of the MoS_2-OH bilayer structure.

Besides sapphire and amorphous SiO_2 substrates, we also successfully grew high-quality monolayer MoS_2 on Si, quartz, SiC, graphene and mica (**Figure S5a - e**). Analogous to sapphire and SiO_2, MoS_2 samples grown on the above substrates without the participation of -OH displayed smaller domain sizes and multilayer structure (**Figure S5-i**). To one's expectation, large-scale MoS_2-OH surface was obtained on those substrates when introducing KOH (**Figure**

S5-ii). The typical Raman spectra all show the Δ ~20 cm^{-1} (**Figure S 5f - j**), demonstrating the monolayer MoS_2 nature.

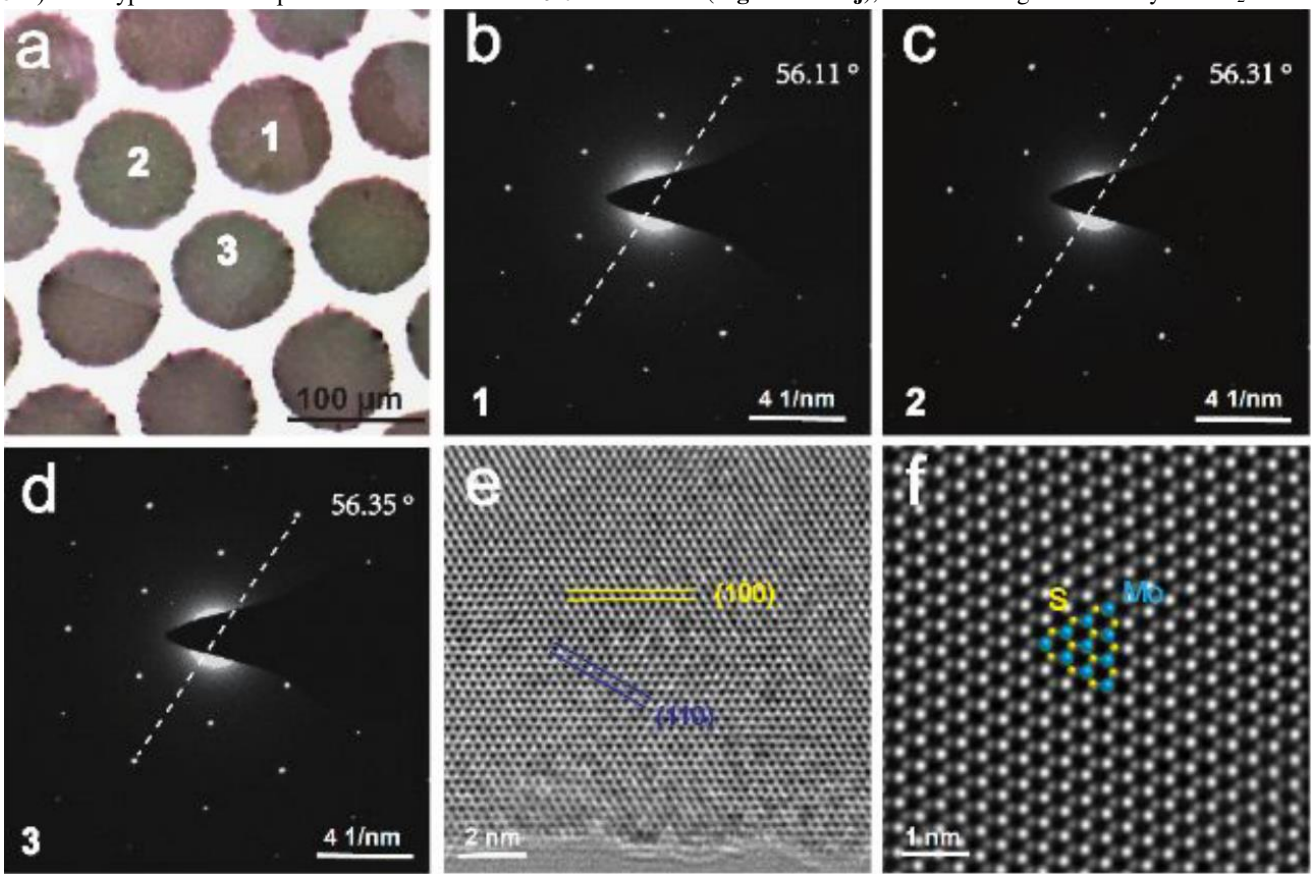

Figure 4. Microstructural characterization of monolayer single-crystal MoS_2 domains. (a) OM image of a side length ~ 150 μm monolayer MoS_2 domain transferred on a TEM grid. (b - d) SAED patterns taken from the areas labelled 1, 2, 3 in **a**, the dashed lines indicate the rotation angles (56.11°, 56.31°, and 56.35°) from the horizontal direction, displaying a single-crystalline lattice structure of the monolayer MoS_2. (e) Aberration-corrected HRTEM image. (f) aberration-corrected ADF-STEM image of monolayer MoS_2, the bright and gray spots correspond to molybdenum and two stacked sulfur atoms, respectively.

In addition, to investigate the influence of different KOH concentrations on the growth, we also grew MoS_2 films with 0.25 and 4 M KOH. MoS_2 grown on sapphire with 0.25 M KOH shows the side length of the triangular domain of ~ 50 μm (**Figure S6a**), and zoomed-in AFM image of the edge shows an irregular terrace structure. It is believed that the amount of -OH is insufficient to cover the upper S atom layer, leading to the partial growth of monolayer. When the concentration of [OH] was further increased to 4 M, the as-grown monolayer MoS_2 domains show side length of ~ 40 μm (**Figure S6b**). Likewise, multilayer and monolayer MoS_2 domains were crystalized on SiO_2 with 0.25 and 4 M KOH, respectively (**Figure S6c and d**). However, the excess of -OH can etch the surface of SiO_2 substrate at 750 ˚C, resulting in small holes (**Figure S6d**). Therefore, the appropriate amount of -OH (1 M KOH) determines high-quality growth of monolayer MoS_2.

In situ transmission electron microscopy (TEM) was used to reveal the dynamic behavior of low-dimensional materials with high spatial and temporal resolution.[35-37] We used a heating stage with a Si_3N_4 membrane inside the TEM to *in situ* observe the dynamic crystallization process of MoS_2 (**Figure 3a**). Firstly, the Si_3N_4 membrane was heated from room temperature to 750 ˚C within 5 min. **Figure 3b-e** and Supporting Movie 1 display the evolution of selected-area electron diffraction (SAED) patterns during the crystallization process. From room temperature to 500 ˚C, there was no diffraction pattern (**Figure 3b**), suggesting the precursor was kept at an amorphous state. When the temperature was reached up to 600 ˚C, indistinct diffraction rings emerged in **Figure 3c**. After the Si_3N_4 substrate being heated to 700 ˚C and 750 ˚C, the diffraction rings became clearer and brighter (**Figure 3d and 3e**). Meanwhile, the distinct SAED patterns can be well indexed to MoS_2 structure with the space group of $P6_3/mmc$ (JCPDS card No. 37-1492). The analysis illustrated a very high crystallization rate of the MoS_2 with -OH. In addition, X-ray diffraction is also used to identify the phase and crystallinity of the MoS_2 products grown at different temperatures. MoS_2 samples (**Figure S7)** have poor crystal quality when they were at 500 and 600 ˚C. In contrast, the MoS_2 sample grown at 750 ˚C has high quality crystallinity, in agreement with the above *in situ* observation. When the temperature was kept at 750 ˚C, the dynamic behavior of the increased flake size was clearly recorded and presented in **Figure 3f - i** and Supporting Movie 2. As shown in **Figure 3f**, a MoS_2 nanobelt with size of ~ 100 nm × 35 nm (length by width) was grown. After being maintained at 750 ˚C for 20 s, the nanobelt grew laterally, and the length and width increased to 200 nm and 70 nm, respectively (**Figure 3g**). With further increasing the growth duration, the width of

MoS_2 flake increased to 80 and 100 nm after 40 and 60 s, respectively (**Figure 3h and i**). As a comparison, we grew MoS_2 on Si_3N_4 membrane without the participation of -OH. As shown in **Figure S8a**, at 750 ˚C from 0 to 480 s, the size of a MoS_2 flake was almost unchanged apart from the increased thickness. **Figure S8b** displays the lateral growth of a MoS_2 flake with -OH for extended time. The final size of the MoS_2 flake reached to 600 nm at 750 ˚C for 480 s, which is much larger than ever achieved by *in situ* growth inside TEM.[37-38] These results directly confirmed the critical role of -OH in growth of high-quality monolayers MoS_2.

We also used X-ray photoelectron spectroscopy (XPS) to investigate the chemical composition of the product during the growth process. As shown in **Figure S9a**, binding energy of the Mo $3d_{5/2}$ electron peaks of the samples grown at 500 and 600 ˚C both have the same value of 232.2 eV, corresponding to Mo^{6+}. It means the non-sulfidized MoO_3.[39] Moreover, the binding energy of the S $2p_{3/2}$ peak appears at 168.2 eV, since the sulfurization could not accomplish at temperature below 600 ˚C. Once the growth temperature was reached to 750 ˚C and kept for 5 min, the signal of the Mo $3d_{5/2}$ peak shifts to a lower binding energy at 229.4 eV, indicative of Mo^{4+} (**Figure S9a**). Meanwhile, the S $2p_{1/2}$ and S $2p_{3/2}$ peaks correspondingly located at 163.2 and 162 eV (**Figure S9b**) imply the formation of MoS_2.[40-41] As shown in **Figure S9c**, the binding energy of K 2p peaks remained unchanged during growth, illustrating K^+ did not participate in redox reaction. Accordingly, the chemical equations are derived below:

$$H_2O + 2OH^- + (NH_4)_2MoO_4 + 4S = MoO_3 + 3H_2S + SO_4^{2-} + 2NH_3 \quad < 750\ ^oC$$

$$2MoO_3 + 7S = 2MoS_2 + 3SO_2 \quad \geq 750\ ^oC$$

Additionally, XPS spectra of oxygen atoms in **Figure S9d** are also used to verify the presence of -OH in the MoS_2 product. The MoS_2 sample prepared with 1 M KOH precursor solution possesses O peaks at 532.5 and 530 eV, corresponding to the SiO_2 and -OH bonds, respectively, while the MoS_2 sample grown without KOH only has the O peak came from SiO_2.[42] The presence of -OH in the product demonstrates the MoS_2-OH bilayer structure.

Electron microscopy was used to probe the microstructure of monolayer MoS_2. The OM image of a typical triangular MoS_2 crystal transferred onto a TEM grid is shown in **Figure 4a**. To identify whether the domain is a single-crystal, we carried out a series of SAED measurements on 3 different regions (**Figure 4a**), and all of the hexagonal diffraction spots have the same crystallographic orientations (deviation smaller than ± 0.3°) in **Figure 4b-d**, confirming the single-crystal nature of the as-grown MoS_2 and uniformity across large area of the sample.[43] **Figure 4e** shows representative high-resolution TEM (HRTEM) images of the single-crystal MoS_2 sample. The lattice distances were measured to be ~ 0.274 nm and 0.158 nm, corresponding to the (100) plane (marked as yellow lines) and (110) plane (marked as blue lines), respectively. Specially, aberration-corrected annular dark field scanning transmission electron microscopy (ADF-STEM) measurement was operated at 200 kV to further identify the structure of the as-grown MoS_2. ADF-STEM image (**Figure 4f**) shows a clearly discernible hexagonal symmetry. The bright/dim areas correspond to Mo/S atoms, respectively.[44-46] The uniform intensity difference between the bright and dim spots indicates that there is no sulphur

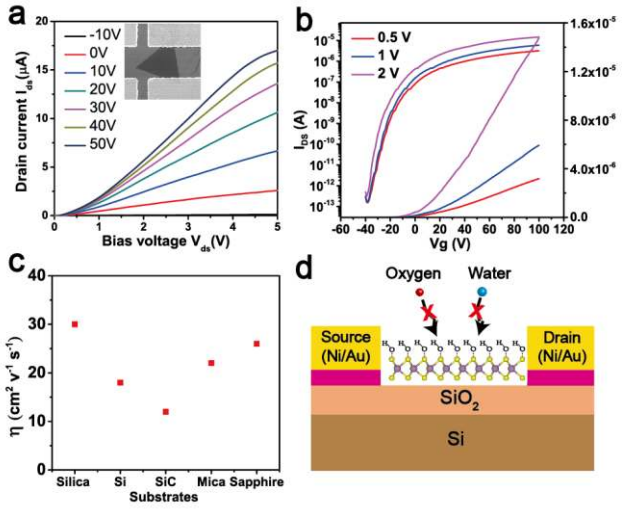

Figure 5. Single-domain MoS_2 FETs. (a) Output characteristics of the device with gate voltages sweeping from −10 to 50 V. Inset: OM image of the device. (b) Transfer characteristics of the device at different V_{DS}. The on/off ratio is ~ 10^7, and $V_{th} \approx$ −35 V. (c) The distributions of the carrier mobility of the MoS_2 FETs based on different substrates. (d) Schematic of the monolayer MoS_2 FET structure. The attached -OH surface layer on the S atom prevents from being oxidized by in air.

vacancy or topological defect. Notably, the high crystal quality and perfect lattice structure benefit from the -OH groups that protect surface S atoms during growth (**Figure 1b**). As a result, the formation of sulphur vacancies and point defects are effectively suppressed.

To evaluate the electrical properties of the resultant monolayer MoS_2, we transferred the MoS_2 monolayer onto clean 300 nm thick SiO_2 (SiO_2/Si) substrates to fabricate back-gate FETs. All the electrical measurements of monolayer MoS_2 were performed in air. A typical device has a channel length (L) of ~ 30 μm and a channel width (W) of ~ 10 μm. **Figure 5a** shows the I-V characteristics of a typical device. The linear curves suggest that ohmic contacts were formed at the source and drain electrodes.[47] The transfer curves in **Figure 5b** show a typical n-type behavior, and the maximum on/off current ratio is > 10^7. The field-effect carrier mobility is estimated using the following equation.

$$\mu = \frac{dI_{ds}}{dV_{bg}} \cdot \frac{L}{WC_iV_{ds}}$$

The carrier mobility was calculated to be as high as 30 $cm^2\ V^{-1}\ s^{-1}$, which is the highest value ever reported in air.[48-50] In addition, **Figure 5c** displays the carrier mobility of FETs based on the monolayer MoS_2 grown on different substrates. The mobility of these devices is in the range of 12 - 30 $cm^2\ V^{-1}\ s^{-1}$. Recent studies have shown that monolayer MoS_2 is prone to be oxidized in air, which can degrade the performance of the devices. To our surprise, the monolayer MoS_2 with surface -OH layer can effectively suppress oxidation in air (**Figure 5d**). Kelvin probe force microscopy (KPFM) images verify that both the as-grown and transferred monolayer MoS_2 keep the MoS_2-OH bilayer structure. The as-grown and transferred monolayer MoS_2 on SiO_2 substrates show almost the same surface potential of ~ 4.65 eV (**Figure S10**). This value is greater than that measured from the mechanically exfoliated MoS_2 due to the presence of -

OH on the surface MoS_2 monolayer.[51-52] This evidence of -OH attachment well agrees with the DFT calculation and XPS measurement (**Figure S9**).

CONCLUSION

In summary, we demonstrated the MoS_2-OH bilayer mediated method for growth of inch-sized monolayer MoS_2 and this method can be applied to various crystalline and amorphous substrates, including sapphire, SiO_2, Si, Si_3N_4, SiC, quartz, mica and graphene. During the crystallization, the -OH groups are attached to the (001) surface of MoS_2, forming a MoS_2-OH bilayer structure. The surface -OH layer not only suspended the growth along the [001] axis and led to preferential growth of MoS_2 monolayers, but also protected the MoS_2 surface from oxidation in air. Moreover, the attached -OH groups on the (001) surface lead to a lower density of sulfur vacancies and defects and enabled the FETs to have the highest electron mobility of MoS_2 in air. The electron microscopy results and high performance of devices both confirmed the high crystalline quality of the monolayer MoS_2. This method provides a new opportunity for the growth of other 2D TMDs such as WS_2, $MoSe_2$, *etc*.

ASSOCIATED CONTENT

Supporting Information

In situ Raman, XPS, TEM, KPFM images of the grown MoS_2. The Supporting Information is available free of charge on the ACS Publications website.

AUTHOR INFORMATION

Corresponding Author

* Corresponding author(s) to whom correspondence should be addressed:

Guifu Zou: zouguifu@suda.edu.cn

Jiang Wu: jiang.wu@ucl.ac.uk

Hongyou Fan: hfan@sandia.gov

Author Contributions

The manuscript was written through contributions of all authors. All authors have given approval to the final version of the manuscript. ‡These authors contributed equally.

ACKNOWLEDGMENT

We appreciate the microscopy analysis from Y. Tang, L. Zhang, and J. Huang from Yanshan University. G.Z. gratefully acknowledges the support from the National Natural Science Foundation of China (21671141),"973 Program - the National Basic Research Program of China" Special Funds for the Chief Young Scientist (2015CB358600), the Priority Academic Program Development (PAPD) of Jiangsu Higher Education Institutions for Optical Engineering in Soochow University; This work was performed, in part, at the Center for Integrated Nanotechnologies (CINT), an Office of Science User Facility operated for the U.S. Department of Energy (DOE) Office of Science by Los Alamos National Laboratory (Contract DE-AC52-06NA25396) and Sandia National Laboratories (Contract DE-NA-0003525). Sandia National Laboratories is a multimission laboratory managed and operated by National Technology and Engineering Solutions of Sandia, LLC., a wholly owned subsidiary of Honeywell International, Inc., for the U.S. Department of Energy's National Nuclear Security Administration under contract DE-NA0003525.

REFERENCES

1. Wang, Q. H.; Kalantar-Zadeh, K.; Kis, A.; Coleman, J. N.; Strano, M. S., Electronics and optoelectronics of two-dimensional transition metal dichalcogenides. *Nat. Nanotech.* **2012,** *7* (11), 699-712.
2. Chhowalla, M.; Shin, H. S.; Eda, G.; Li, L.-J.; Loh, K. P.; Zhang, H., The chemistry of two-dimensional layered transition metal dichalcogenide nanosheets. *Nat. Chem.* **2013,** *5* (4), 263-275.
3. Xia, F.; Wang, H.; Xiao, D.; Dubey, M.; Ramasubramaniam, A., Two-dimensional material nanophotonics. *Nat. Photonics* **2014,** *8* (12), 899-907.
4. Xu, H.; Han, X.; Dai, X.; Liu, W.; Wu, J.; Zhu, J.; Kim, D.; Zou, G.; Sablon, K. A.; Sergeev, A., High Detectivity and Transparent Few-Layer MoS2 /Glassy-Graphene Heterostructure Photodetectors. *Adv. Mater.* **2018,** *30* (13), e1706561.
5. Chen, Y.; Fan, Z.; Zhang, Z.; Niu, W.; Li, C.; Yang, N.; Chen, B.; Zhang, H., Two-Dimensional Metal Nanomaterials: Synthesis, Properties, and Applications. *Chem. Rev.* **2018,** *118* (13), 6409-6455.
6. Akinwande, D.; Petrone, N.; Hone, J., Two-dimensional flexible nanoelectronics. *Nat. Commun.* **2014,** *5*, 5678.
7. Shi, Y.; Li, H.; Li, L.-J., Recent advances in controlled synthesis of two-dimensional transition metal dichalcogenides via vapour deposition techniques. *Chem. Soc. Rev.* **2015,** *44* (9), 2744-2756.
8. Yin, Z.; Li, H.; Li, H.; Jiang, L.; Shi, Y.; Sun, Y.; Lu, G.; Zhang, Q.; Chen, X.; Zhang, H., Single-layer MoS2 phototransistors. *ACS Nano* **2011,** *6* (1), 74-80.
9. Sundaram, R.; Engel, M.; Lombardo, A.; Krupke, R.; Ferrari, A.; Avouris, P.; Steiner, M., Electroluminescence in single layer MoS2. *Nano Lett.* **2013,** *13* (4), 1416-1421.
10. Zhan, Y.; Liu, Z.; Najmaei, S.; Ajayan, P. M.; Lou, J., Large- area vapor- phase growth and characterization of MoS2 atomic layers on a SiO2 substrate. *Small* **2012,** *8* (7), 966-971.
11. Wang, X.; Feng, H.; Wu, Y.; Jiao, L., Controlled synthesis of highly crystalline MoS2 flakes by chemical vapor deposition. *J. Am. Chem. Soc.* **2013,** *135* (14), 5304-5307.
12. Wei, C.; Jing, Z.; Jing, Z.; Lin, G.; Yang, Z.; Li, X.; Hua, Y.; Zhu, X.; Rong, Y.; Shi, D., Oxygen-Assisted Chemical Vapor Deposition Growth of Large Single-Crystal and High-Quality Monolayer MoS2. *J. Am. Chem. Soc.* **2015,** *137* (50), 15632-15635.
13. Zhang, Z.; Chen, P.; Duan, X.; Zang, K.; Luo, J.; Duan, X., Robust epitaxial growth of two-dimensional heterostructures, multiheterostructures, and superlattices. *Science* **2017,** *357* (6353), 788-792.
14. Chen, J.; Zhao, X.; Tan, S. J.; Xu, H.; Wu, B.; Liu, B.; Fu, D.; Fu, W.; Geng, D.; Liu, Y., Chemical Vapor Deposition of Large-Size Monolayer MoSe 2 Crystals on Molten Glass. *J. Am. Chem. Soc.* **2017,** *139* (3), 1073-1076.
15. Yang, P.; Zou, X.; Zhang, Z.; Hong, M.; Shi, J.; Chen, S.; Shu, J.; Zhao, L.; Jiang, S.; Zhou, X., Batch production of 6-inch uniform monolayer molybdenum disulfide catalyzed by sodium in glass. *Nat. Commun.* **2018,** *9* (1), 979.
16. Yu, Y.; Li, C.; Liu, Y.; Su, L.; Zhang, Y.; Cao, L., Controlled Scalable Synthesis of Uniform, High-Quality Monolayer and Few-layer MoS2 Films. *Sci. Rep.* **2013,** *3*, 1866.
17. Chen, J.; Zhao, X.; Tan, S. J.; Xu, H.; Wu, B.; Liu, B.; Fu, D.; Fu, W.; Geng, D.; Liu, Y.; Liu, W.; Tang, W.; Li, L.; Zhou, W.; Sum, T. C.; Loh, K. P., Chemical Vapor Deposition of Large-Size Monolayer MoSe2 Crystals on Molten Glass. *J Am Chem Soc* **2017,** *139* (3), 1073-1076.
18. Shi, J.; Zhang, X.; Ma, D.; Zhu, J.; Zhang, Y.; Guo, Z.; Yao, Y.; Ji, Q.; Song, X.; Zhang, Y., Substrate facet effect on the

growth of monolayer MoS2 on Au foils. *ACS Nano* **2015,** *9* (4), 4017-4025.

19. Gao, Y.; Liu, Z.; Sun, D. M.; Huang, L.; Ma, L. P.; Yin, L. C.; Ma, T.; Zhang, Z.; Ma, X. L.; Peng, L. M.; Cheng, H. M.; Ren, W., Large-area synthesis of high-quality and uniform monolayer WS2 on reusable Au foils. *Nat Commun* **2015,** *6*, 8569.

20. Blöchl, P. E., Projector augmented-wave method. *Phys. Rev. B* **1994,** *50* (24), 17953.

21. Perdew, J. P.; Burke, K.; Ernzerhof, M., Generalized gradient approximation made simple. *Phys. Rev. Lett.* **1996,** *77* (18), 3865-3868.

22. Kresse, G.; Joubert, D., From ultrasoft pseudopotentials to the projector augmented-wave method. *Phys. Rev. B* **1999,** *59* (3), 1758-1775.

23. Kresse, G.; Furthmüller, J., Efficient iterative schemes for ab initio total-energy calculations using a plane-wave basis set. *Phys. Rev. B* **1996,** *54* (16), 11169-11186.

24. Grimme, S., Semiempirical GGA- type density functional constructed with a long- range dispersion correction. *J. Comput. Chem.* **2006,** *27* (15), 1787-1799.

25. Lodziana, Z.; Norskov, J.; Stoltze, P., The stability of the hydroxylated (0001) surface of alpha-Al2O3. *J. Chem. Phys.* **2003,** *118* (24), 11179-11188.

26. Grosjean, B.; Pean, C.; Siria, A.; Bocquet, L.; Vuilleumier, R.; Bocquet, M.-L., Chemisorption of hydroxide on 2D materials from DFT calculations: graphene versus hexagonal boron nitride. *J. Phys. Chem. Lett.* **2016,** *7* (22), 4695-4700.

27. Takeda, S.; Fukawa, M.; Hayashi, Y.; Matsumoto, K., Surface OH group governing adsorption properties of metal oxide films. *Thin Solid Films* **1999,** *339* (1-2), 220-224.

28. Lee, C.; Yan, H.; Brus, L. E.; Heinz, T. F.; Hone, J.; Ryu, S., Anomalous lattice vibrations of single-and few-layer MoS2. *ACS Nano* **2010,** *4* (5), 2695-2700.

29. Liu, K.; Zhang, L.; Cao, T.; Jin, C.; Qiu, D.; Zhou, Q.; Zettl, A.; Yang, P.; Louie, S. G.; Wang, F., Evolution of interlayer coupling in twisted molybdenum disulfide bilayers. *Nat. Commun.* **2014,** *5*, 4966.

30. Liu, K. K.; Zhang, W.; Lee, Y. H.; Lin, Y. C.; Chang, M. T.; Su, C. Y.; Chang, C. S.; Li, H.; Shi, Y.; Zhang, H., Growth of large-area and highly crystalline MoS2 thin layers on insulating substrates. *Nano Lett.* **2012,** *12* (3), 1538-1544

31. Gong, Y.; Ye, G.; Lei, S.; Shi, G.; He, Y.; Lin, J.; Zhang, X.; Vajtai, R.; Pantelides, S. T.; Zhou, W., Synthesis of Millimeter- Scale Transition Metal Dichalcogenides Single Crystals. *Adv. Funct. Mater.* **2016,** *26* (12), 2009-2015.

32. Gurarslan, A.; Yu, Y.; Su, L.; Yu, Y.; Suarez, F.; Yao, S.; Zhu, Y.; Ozturk, M.; Zhang, Y.; Cao, L., Surface-energy-assisted perfect transfer of centimeter-scale monolayer and few-layer MoSâ‚‚ films onto arbitrary substrates. *ACS Nano* **2014,** *8* (11), 11522-11528.

33. Pütz, J.; Aegerter, M. A., MoS x Thin Films by Thermolysis of a Single-Source Precursor. *J. Sol-gel Sci. Technol.* **2000,** *19* (1-3), 821-824.

34. Liu, K. K.; Zhang, W.; Lee, Y. H.; Lin, Y. C.; Chang, M. T.; Su, C. Y.; Chang, C. S.; Li, H.; Shi, Y.; Zhang, H., Growth of Large-Area and Highly Crystalline MoS2 Thin Layers on Insulating Substrates. *Nano Letters* **2012,** *12* (3), 1538.

35. Fei, L.-f.; Sun, T.-y.; Lu, W.; An, X.-q.; Hu, Z.-f.; Jimmy, C. Y.; Zheng, R.-k.; Li, X.-m.; Chan, H. L.; Wang, Y., Direct observation of carbon nanostructure growth at liquid–solid interfaces. *Chem. Commun.* **2014,** *50* (7), 826-828.

36. Ramachandramoorthy, R.; Bernal, R.; Espinosa, H. D., Pushing the envelope of in situ transmission electron microscopy. *ACS Nano* **2015,** *9* (5), 4675-4685.

37. Fei, L.; Lei, S.; Zhang, W.-B.; Lu, W.; Lin, Z.; Lam, C. H.; Chai, Y.; Wang, Y., Direct TEM observations of growth mechanisms of two-dimensional MoS 2 flakes. *Nat. Commun.* **2016,** *7*, 12206.

38. Zink, N.; Therese, H. A.; Pansiot, J.; Yella, A.; Banhart, F.; Tremel, W., In situ heating TEM study of onion-like WS2 and MoS2 nanostructures obtained via MOCVD. *Chem. Mater.* **2007,** *20* (1), 65-71.

39. Swiatowska-Mrowiecka, J.; de Diesbach, S.; Maurice, V.; Zanna, S.; Klein, L.; Briand, E.; Vickridge, I.; Marcus, P., Li-ion intercalation in thermal oxide thin films of MoO3 as studied by XPS, RBS, and NRA. *J. Phys. Chem. C* **2008,** *112* (29), 11050-11058.

40. Baker, M.; Gilmore, R.; Lenardi, C.; Gissler, W., XPS investigation of preferential sputtering of S from MoS2 and determination of MoSx stoichiometry from Mo and S peak positions. *Appl. Surf. Sci.* **1999,** *150* (1-4), 255-262.

41. Li, Y.; Wang, H.; Xie, L.; Liang, Y.; Hong, G.; Dai, H., MoS2 Nanoparticles Grown on Graphene: An Advanced Catalyst for the Hydrogen Evolution Reaction. *J. Am. Chem. Soc.* **2011,** *133* (19), 7296-7299.

42. McCafferty, E.; Wightman, J., Determination of the concentration of surface hydroxyl groups on metal oxide films by a quantitative XPS method. *Surf. Interface Anal.* **1998,** *26* (8), 549-564.

43. Gao, L.; Ren, W.; Xu, H.; Li, J.; Wang, Z.; Teng, M.; Ma, L. P.; Zhang, Z.; Qiang, F.; Peng, L. M., Repeated growth and bubbling transfer of graphene with millimetre-size single-crystal grains using platinum. *Nat. Commun.* **2012,** *3* (2), 699.

44. Lee, Y. H.; Zhang, X. Q.; Zhang, W.; Chang, M. T.; Lin, C. T.; Chang, K. D.; Yu, Y. C.; Wang, J. T. W.; Chang, C. S.; Li, L. J., Synthesis of large- area MoS2 atomic layers with chemical vapor deposition. *Adv. Mater.* **2012,** *24* (17), 2320-2325.

45. Najmaei, S.; Liu, Z.; Zhou, W.; Zou, X.; Shi, G.; Lei, S.; Yakobson, B. I.; Idrobo, J.-C.; Ajayan, P. M.; Lou, J., Vapour phase growth and grain boundary structure of molybdenum disulphide atomic layers. *Nat. Mater.* **2013,** *12* (8), 754-759.

46. Hong, J.; Hu, Z.; Probert, M.; Li, K.; Lv, D.; Yang, X.; Gu, L.; Mao, N.; Feng, Q.; Xie, L., Exploring atomic defects in molybdenum disulphide monolayers. *Nat. Commun.* **2015,** *6*, 6293.

47. Das, S.; Chen, H.-Y.; Penumatcha, A. V.; Appenzeller, J., High performance multilayer MoS2 transistors with scandium contacts. *Nano Lett.* **2012,** *13* (1), 100-105.

48. Qiu, H.; Pan, L.; Yao, Z.; Li, J.; Shi, Y.; Wang, X., Electrical characterization of back-gated bi-layer MoS2 field-effect transistors and the effect of ambient on their performances. *Appl. Phys. Lett.* **2012,** *100* (12), 123104-123107.

49. Lee, S. Y.; Kim, U. J.; Chung, J.; Nam, H.; Jeong, H. Y.; Han, G. H.; Kim, H.; Oh, H. M.; Lee, H.; Kim, H., Large work function modulation of monolayer MoS2 by ambient gases. *ACS Nano* **2016,** *10* (6), 6100-6107.

50. Cho, K.; Park, W.; Park, J.; Jeong, H.; Jang, J.; Kim, T.-Y.; Hong, W.-K.; Hong, S.; Lee, T., Electric stress-induced threshold voltage instability of multilayer MoS2 field effect transistors. *ACS Nano* **2013,** *7* (9), 7751-7758.

51. Li, D.; Xiao, Z.; Mu, S.; Wang, F.; Liu, Y.; Song, J.; Huang, X.; Jiang, L.; Xiao, J.; Liu, L.; Ducharme, S.; Cui, B.; Hong, X.; Jiang, L.; Silvain, J. F.; Lu, Y., A Facile Space-Confined Solid-Phase Sulfurization Strategy for Growth of High-Quality Ultrathin Molybdenum Disulfide Single Crystals. *Nano Lett* **2018,** *18* (3), 2021-2032.

52. Ochedowski, O.; Marinov, K.; Scheuschner, N.; Poloczek, A.; Bussmann, B. K.; Maultzsch, J.; Schleberger, M., Effect of contaminations and surface preparation on the work function of single layer MoS2. *Beilstein J. Nanotechnol.* **2014,** *5*, 291-297.

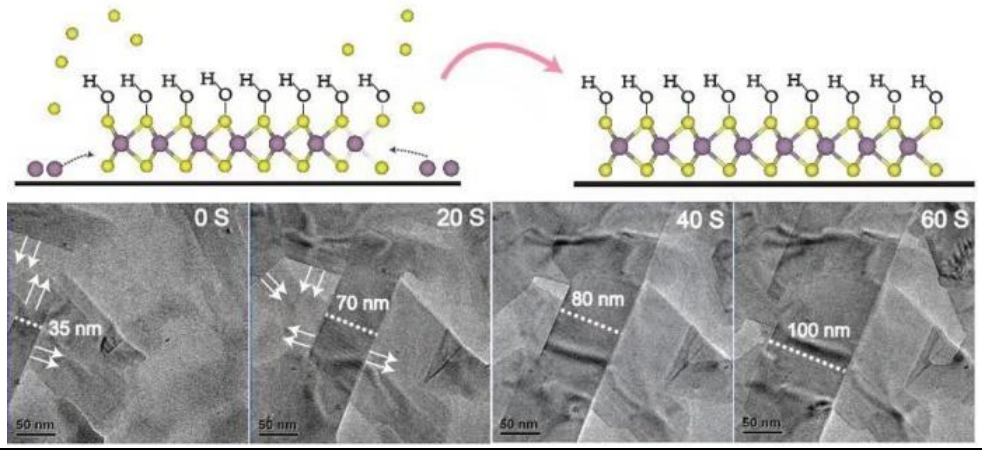
0 S
35 nm
50 nm
20 S
70 nm
50 nm
40 S
80 nm
50 nm
60 S
100 nm
50 nm